Boosting the terahertz nonlinearity of graphene by orientation disorder

To cite this article before publication: Baek et al, 2017, 2D Mater., at press:
http://dx.doi.org/10.1088/2053-1583/aa5c64

Boosting the terahertz nonlinearity of graphene by orientation disorder

I H Baek[1,6], J M Hamm[2], K J Ahn[1], B J Kang[1], S S Oh[2], S Bae[3], S Y Choi[1], B H Hong[4], D-I Yeom[1], B Min[5], O Hess[2], Y U Jeong[6] and F Rotermund[1,7]

[1]Department of Physics and Department of Energy Systems Research, Ajou University, Suwon 443-749, Republic of Korea
[2]The Blackett Laboratory, Department of Physics, Imperial College London, London SW7 2AZ, United Kingdom
[3]Soft Innovative Materials Research Center, Korea Institute of Science and Technology, Wanju-gun 565-905, Republic of Korea
[4]Department of Chemistry, Seoul National University, Seoul 151-747, Republic of Korea
[5]Department of Mechanical Engineering, Korea Advanced Institute of Science and Technology, Daejeon 34141, Republic of Korea
[6]Center for Quantum Beam-based Radiation Research, Korea Atomic Energy Research Institute, Daejeon 305-353, Republic of Korea
[7]Department of Physics, Korea Advanced Institute of Science and Technology, Daejeon 34141, Republic of Korea

E-mail: rotermund@kaist.ac.kr

Abstract. The conical band structure is the cornerstone of graphene's ultra-broadband optical conductivity. For practical use of graphene in nonlinear photonics, however, substantial increases of the light-matter interaction strength will be required while preserving the promising features of monolayers, as the interaction of light with a single atomic layer is limited due to the extremely short interaction length and low density of state, particularly for the long-wavelength region. Here, we report that this demand can be fulfilled by random stacking of high-quality large-area monolayer graphene up to a requested number of layers, which leads to the electronic interaction between layers being effectively switched off due to turbostratic disorder. The nonlinear characteristics of randomly stacked multilayer graphene (RSMG), which originates from a thermo-modulational feedback mechanism through ultrafast free-carrier heating and temperature-dependent carrier-phonon collisions, show clear improvements in the terahertz (THz) regime with increasing layer numbers, whereas as-grown multilayer graphene (AGMG) exhibits limited behaviors due to strong interlayer coupling. This controllable nonlinearity enhancement provides an ideal prerequisite for developing efficient graphene-based THz photonic devices.

Keywords. Graphene, Random stacking, Terahertz nonlinearity, Ultrafast terahertz conductivity, Terahertz nonlinear absorption

1. Introduction

Since the demonstration of the successful isolation of a single atomic layer of carbon, i.e., graphene, from bulk graphite, the electronic transport and optical properties of graphene have been intensively exploited [1-5]. Subsequent studies on various nonlinear optical phenomena of graphene, such as

nonlinear absorption [6-8], optical limiting [9,10], and optical frequency conversion [11,12], have been conducted by employing ultrashort laser pulses. In addition, intraband relaxation and interband recombination dynamics in graphene were investigated by optical pump and THz probe spectroscopy [13]. However, these intrinsic nonlinearities of graphene in visible and near-infrared frequency ranges are still considered to be limited for practical photonic applications [14]. Furthermore, fabricating high-quality monocrystalline graphene on a wafer scale remains extremely difficult even with the current state-of-the-art technology.

Despite these issues, however, the nonlinear optical application of graphene in the terahertz (THz) frequency regime appears highly promising, since the highly doped monolayer graphene and nearly intrinsic multilayer graphene can substantially absorb THz photons through intraband [15,16] and interband transitions [17]. Recent theoretical and experimental studies have demonstrated that a recorded photon absorption rate of up to 46% and a transmission modulation reaching 28% could be achieved by moderate fluences of THz pulses [18-20]. Furthermore, many of these results were obtained by using polycrystalline graphene fabricated by chemical vapor deposition (CVD), indicating that the THz nonlinear properties are not significantly influenced by the preferential direction of graphene's crystallinity due to the relatively long wavelengths of THz pulses (λ=300 μm at 1 THz) compared to the typical average domain size (~ a few micrometers) of the graphene samples used.

In addition to the promising THz nonlinearity of monolayer graphene, the improved functionality required by practical applications can be obtained by fabricating multilayer graphene. Although recent studies on the interlayer interaction in bilayer graphene have shown that Van Hove singularities in the electronic band structure of bilayer graphene could be effectively switched on/off by rotating the relative orientation between two graphene layers [21,22], the impact of this effect on the THz frequency regime appears to be limited, as this single domain feature is mainly smeared by the multi-domain nature of graphene on a scale of a few centimeters.

In this study, we prepared four graphene samples with different numbers of layers on a wafer scale to investigate their THz nonlinearities through nonlinear transmission and z-scan experiments with high-

intensity broadband THz pulses centered at 0.6 THz (see Experimental Section). Large-area multilayer graphene samples of high quality could be prepared by the sequential random stacking of monolayer graphene up to the required number of layers. The key difference between our RSMG devices and the devices consisted of the same number of individual monolayer graphene is that two neighboring layers in RSMG films are not separated by a spacer but connected by a weak interlayer van der Waals force on atomic scales. This electronic interaction between layers can be effectively switched off in THz nonlinear devices due to turbostratic disorder of CVD-grown graphene layers, which leads to preserving the Dirac-fermionic feature of graphene and, in eventual, is responsible for the observed enhanced nonlinearities of RSMG films with a few atomic thicknesses. In nonlinear transmission experiments, we obtained more than four-fold enhancement in transmission modulation with a 4-layer RSMG compared to an AGMG with the same number of layers. Through the excellent agreement of experimental results with a theoretical model, we are able to explain the observed nonlinear transmission modulation of our samples based on a thermo-modulational feedback mechanism whereby the optical conductivity of graphene is driven by the ultrafast heating of carriers and carrier-phonon collisions which affect the absorptivity during the passage of a high-intensity THz pulse. From z-scan experimental results, we confirmed that the nonlinear absorption coefficients of RSMGs in the THz frequency region are one order of magnitude larger than those of AGMGs and even three orders of magnitude larger than the values measured in the near-IR spectral range.

2. Raman spectroscopic responses of AGMGs and RSMGs

Monolayer graphene can be synthesized by CVD growth on large-area Cu foils. Figure 1a shows a photograph of acentrically stacked monolayer graphene layers in dimensions of 2×2 cm^2. In addition to a monolayer sample, 2-, 4-, and 8-layer graphene samples were fabricated by iterative transfer processes on quartz substrates (see inset and Experimental Section). In our multilayer graphene samples, the interlayer orientation cannot be sharply defined, as the crystal axes of monocrystalline domains on the order of few tens of micron square are randomly oriented in the stacked area [23,24]. In addition to RSMG samples, we fabricated AGMG samples, which were directly synthesized by

controlling CVD conditions without further additional stacking procedures, to compare the nonlinear optical characteristics between the two arrangements. The measured UV-to-NIR transmission spectra (see Section S1 of Supplementary Information (SI)) confirmed that these AGMG films consisted of two and four graphene layers, with 2.3% absorption per layer, as governed by the fine structure constant ($\alpha = e^2/(4\pi\hbar\varepsilon_0 c) \approx 1/137$).

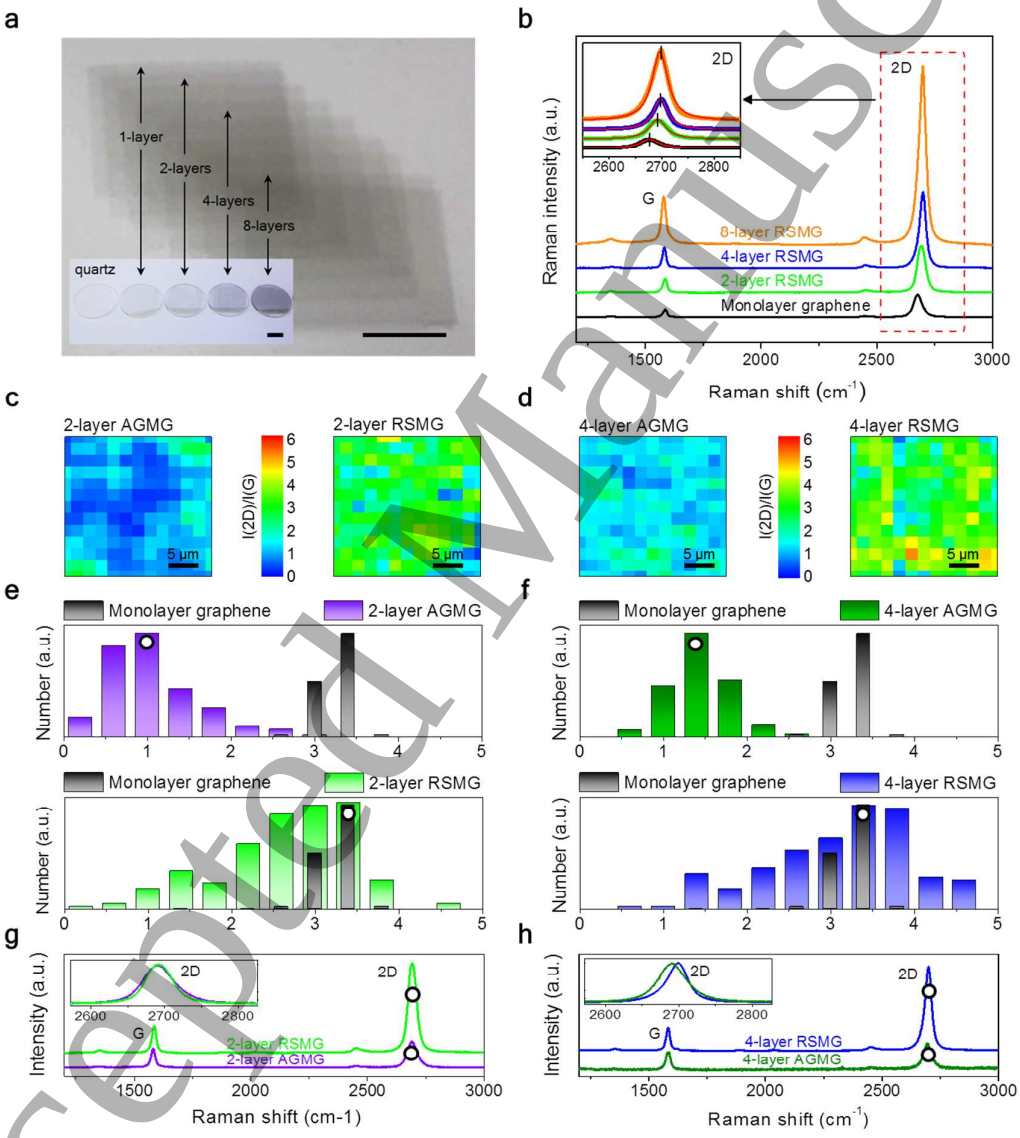

Figure 1. Photographs and Raman characteristics of RSMGs and AGMGs. (a) Photographs of step-like RSMGs and graphene films transferred onto quartz substrates for experiments (inset). The different opacities in the overlapping regions are visible to the naked eye (scale bars are 1 cm). (b) Raman spectra of four RSMGs at 514 nm excitation. G-peaks and 2D-peaks appear at approximately 1582 and 2690 cm^{-1}, respectively, corresponding to the E_{2g} vibration mode at the Γ-point the second-order A_{1g} phonon vibration mode at the K-point in

momentum space. The inset magnifies the region around the 2D-modes. Vertical lines imply the blue-shift of 2D-mode frequencies after stacking processes. (c-f) Two-dimensional mapping data (13 × 13 points over the area of 25 × 25 μm^2) and their statistic analyses for Raman spectra of four different multilayer graphene samples. The relative peak intensities of the 2D-mode with respect to that of the G-mode (I(2D)/I(G)) are differentially distributed depending on the stacked structure and the number of graphene layers. For a comparison, the relative peak intensity distribution of monolayer graphene is also shown in four histograms with black histogram. (g,h) Raman spectra measured at several sampling points (circles in Figure 1e and 1f). The Lorentzian FWHM (39.8 cm^{-1}) of the 2D-mode in monolayer graphene was retained even after the stacking process in RSMGs (37.7 ± 3.6 cm^{-1}), whereas the FWHMs of the 2-layer and 4-layer AGMGs were broadened to 45.2 and 41.9 cm^{-1} (see insets).

Raman spectroscopy measurements were conducted with a commercial Raman microscope (inVia Raman microscope, Renishaw plc. Gloucestershire, UK) to examine the crystalline quality of the samples and assess the number of layers and stacking order. A light at a wavelength of 514 nm was focused on graphene samples (a focused spot size ~ 1 μm^2) using an objective lens (Numerical Aperture = 0.5, 20X). For each sample, Raman spectra were performed at 169 (13 × 13) different points in area of 25 × 25 μm^2.

We measured intensities at the G- (1582 cm^{-1}) and the 2D-mode (2690 cm^{-1}) in Raman spectra and presented the spatial mappings of the 2D-peak intensity normalized by the G-peak intensity (I(2D)/I(G)) in figure 1c and 1d. Figure 1e and 1f show their statistical analysis. The values of I(2D)/I(G) are mostly distributed from 0 to 6 for all samples, but their average values and distributions are apparently different from each other, depending on the number of layer and the stacking method. For an easy comparison, the I(2D)/I(G) distribution of monolayer graphene (black histograms) reported in our previous work are presented as well [25]. We observed clear differences in Raman responses between AGMGs and RSMGs. In case of AGMG samples, the peak intensities of the 2D-mode at whole locations are nearly analogous to those of the G-mode or slightly higher. This result seems to be quite similar to typical Raman responses of Bernal stacked 2-layer graphene [26]. The 2D-mode in monolayer graphene splits into four different modes in Bernal stacked 2-layer graphene due to the double resonance process of the optical phonons. As a consequence, the value of I(2D)/I(G) decreases in AGMG [21]. By contrast, the value of I(2D)/I(G) for RSMGs show widespread

distributions, and the most of locations of RSMGs show similar characteristics of monolayer graphene. From these Raman spectroscopic data, we selected the most representative Raman spectra of our graphene samples and found that the iterative layer-by-layer stacking process led to only marginal changes in the Raman spectra (see figure 1b). While the peak intensity of the G- and 2D-modes increased linearly with an increasing number of layers, the relative peak intensity I(2D)/I(G) was nearly constant (~3) for all samples. The almost suppressed D-mode at approximately 1350 cm^{-1} and the Lorentzian-shape of the 2D-mode at approximately 2690 cm^{-1} (see inset) are two clear indicators of the high quality of graphene and the stacking orientation disorder of the fabricated samples [27]. From the frequency shift of the G-mode located near 1580 cm^{-1}, which is linked to the stretching mode of C-C bonding and directly correlates with the doping state of graphene [28-30], we found that all fabricated RSMG samples are *p*-doped with a Fermi level of about -162 meV. From the quasi-maintained line shapes at both modes, all RSMG samples can be considered to possess nearly the same electronic band structure of monolayer graphene, except for the degeneracy of the electronic states. Since crystalline species of graphene can be also identified by spectral bandwidth of the 2D-mode, we compared Raman spectra (see figure 1g and 1h) at several selected sampling points in four histograms and found that the 2- and 4-layer AGMG samples have broader full widths at half maximum (FWHM) at the 2D mode (45.2 and 41.9 cm^{-1}) than the monolayer graphene (39.8 cm^{-1}) or RSMG (36.7 cm^{-1}). From the fact that the Raman response of RSMGs shows a clear similarity to that of monolayer graphene in shape and distribution, we expect that the nonlinear optical characteristics of graphene in the THz regime could be well preserved even in multilayer graphene films, when individual graphene sheets are artificially stacked, not naturally grown.

3. THz nonlinear transmission characteristics of AGMG and RSMG and thermo-modulational feedback model

To confirm the influence of the number of layers (*N*) and the interlayer coupling on the THz nonlinear conductivities of RSMG and AGMG samples, the intensity-dependent THz transmission behaviors were investigated (figure 2; see also Section 2 of SI for the detailed transmission-type THz nonlinear

spectroscopy system). We observed clear distinctions in THz absorption and nonlinear transmission modulation between the RSMGs and AGMGs, as shown in figure 2a. In the lower THz fluence regime < 100 nJ/cm^2, the linear THz transmissions (T_{lin}) of RSMG samples were measured to be approximately 71% (2-layer) and 55% (4-layer), and these results are nearly analogous to linear THz transmission data measured by a THz-TDS (time-domain spectroscopy) using a photoconductive antenna based on a Ti:sapphire oscillator (see Figure S1b of SI). In case of AGMG samples, T_{lin} are measured to be 76% for the 2-layer and 69% for the 4-layer. The measured T_{lin} and Raman G-mode frequencies (~1582 cm^{-1} for both AGMGs in figure 1c and 1d) indicate that chemical potentials of AGMG samples are comparable to those of RSMG samples [30].

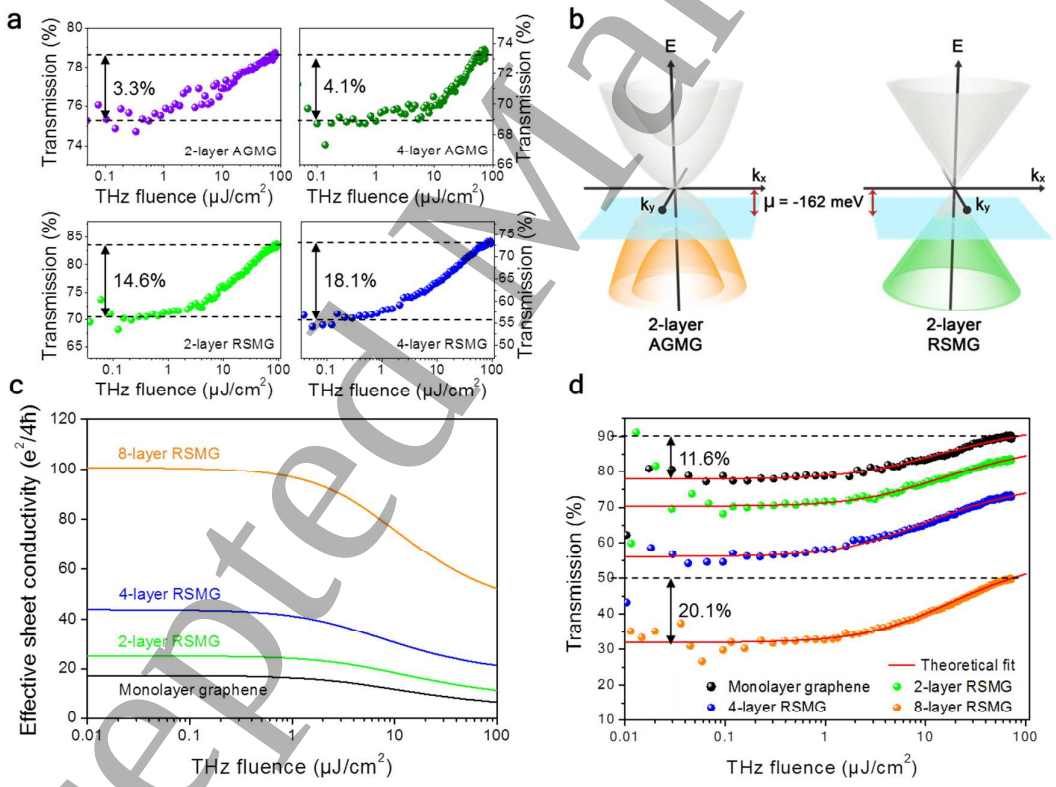

Figure 2. Nonlinear optical characteristics of RSMGs and AGMGs in THz frequency range. (a) THz nonlinear transmission of RSMG and AGMG films depends on the number of active bands for the occupied level of carriers. (b) Schematics of different electronic band structures of 2-layer AGMG and RSMG. (c) Effective sheet conductivity of four RSMGs as a function of incident THz fluence. (d) Experimental results on change in nonlinear THz transmission (dots) for monolayer graphene and 2-, 4- and 8-layer RSMGs as a function of

incident THz fluence, together with theoretical fits obtained from thermo-modulational pulse-transmission theory (red solids).

As the THz fluence increased above 1 μJ/cm^2, all of the samples became gradually transparent. The THz nonlinear modulation depth (ΔT), defined as the transmission difference between the saturated transmission (T_{sat}) at a THz fluence of 85.5 μJ/cm^2 and the linear one (T_{lin}), was measured to be approximately four times larger for a RSMG sample than an AGMG sample with the same number of layers (*N=2* and *4*).

The enhanced THz nonlinear modulation of RSMGs is attributed to the increased number of active bands that interact with incoming THz photons, as shown in figure 2b (see Section 3 in SI for detailed discussion). At a measured chemical potential of μ=-162 meV, the number of active bands in an AGMG is always smaller than in an equivalent RSMG. As a consequence, AGMGs possess lower THz conductivities than RSMGs. For instance, in the 2-layer AGMG, half of the electronic bands do not contribute to the THz conductivity because the interlayer coupling raises the sub-lattice symmetry near the K-point and pushes down the lowest valence band by as much as ~0.4 eV, assuming both layers to be AB-stacked with an electron-hole asymmetry [31,32]. The values of T_{lin} and ΔT of the 4-layer AGMG can be explained similarly. By contrast, the *N*-fold degenerate bands in RSMGs are all active and retain the linear dispersion of the monolayer graphene. As a result, the THz conductivity of a RSMG grows stronger as the number of graphene layers *N* increases, as shown in figure 2c.

The observed nonlinearities of our graphene are explained by the intraband (ohmic) heating of the carrier plasma caused by intense THz fields, which in turn induces a change of carrier temperature and collision loss during the passage of the pulse [17,19,20,33]. The resulting change of conductivity on sub-picosecond timescales [19] leads to a saturation of pulse transmission with increasing THz fluence. To account for the differential changes of temperature and collision loss during the passage of the pulse we formulate a thermo-modulational pulse-transmission model detailed in Section 5 of the SI.

Figure 2d shows the measured THz nonlinear transmission data for our RSMG samples with different numbers of layers (circles) and the corresponding theoretical calculations (solid lines), where the THz

modulation depths of monolayer graphene and 2-, 4-, and 8-layer RSMG were measured to be 11.6%, 14.6%, 18.1%, and 20.1%, respectively. In our theoretical model, as RSMGs retain the linear band structure of a graphene monolayer, the effective conductivity of a *N*-layer graphene is simply expressed by $N\sigma_1(\mu, \theta; \gamma_{coll})$, where σ_1 is the conductivity of monolayer graphene depending on the chemical potential μ, carrier temperature θ, and collision rate γ_{coll} [33]. During the passage of a THz pulse (~1 ps), the pulse energy is continuously transferred to the carrier plasma by collective excitation of the electrons in the valence band, leading to an increase in carrier temperature θ and, eventually, a higher collision rate γ_{coll} (see Section S4 in SI), which in turn decreases the intraband conductivity, as shown in figure 2c. In addition to the excellent agreement between the theoretical and experimental values, we found that the values of the efficiency parameter η, the fraction of the absorbed energy remaining in the carrier system over the duration of the pulse, are of the same order of magnitude as those reported in a previous THz-pump/THz-probe experiment [34] (see Section 5 in SI for a detailed discussion).

4. THz nonlinear absorption coefficients of AGMG and RSMG measured by z-scan

The nonlinearity of RSMG can be further quantified by the nonlinear absorption coefficient (β_{THz}). Open-aperture THz z-scan measurements were performed on graphene samples. Figure 3a shows that the highest THz peak intensity at the focus (~19.6 MW/cm^2) between two off-axis parabolic mirrors leads to an increase of the THz transmission in all graphene samples. The β_{THz} values obtained for monolayer and 2-, 4-, and 8-layer RSMG samples were -1.76 × 10^4, -1.26 × 10^4, -1.01 × 10^4, -0.67 × 10^4 cm/MW, respectively, extracted by standard z-scan fitting equations [35]. Despite the slight decrease in β_{THz} with increasing *N* resulting from contamination with a residual polymer and ambiguous defects during the stacking process, these values were of the same order of magnitude as the values derived from the thermo-modulational transmission model, -9.94 × 10^4, -6.16 × 10^4, -4.63 × 10^4, and -3.94 × 10^4 cm/MW, respectively. For 2- and 4-layer AGMG samples, β_{THz} values (-3.81 × 10^3 and -1.49× 10^3 cm/MW) are one order lower than those of RSMG for the same *N* due to the reduced density of states in AGMG. All β_{THz} values of RSMG samples in the THz regime are

approximately three orders of magnitude lager than the values measured at a wavelength of 800 nm (-3.06 × 10^1, -1.87 × 10^1, -1.29 × 10^1, and -1.10 × 10^1 cm/MW for the mono-, 2-, 4-, and 8-layer graphene, respectively; see also figure S6 in the SI). To show the reliability of measurements, we depict the values of our samples together with the previously reported values for monolayer and 2-layer graphenes [8,36] and other low-dimensional nanocarbons [37,38] in figure 3b.

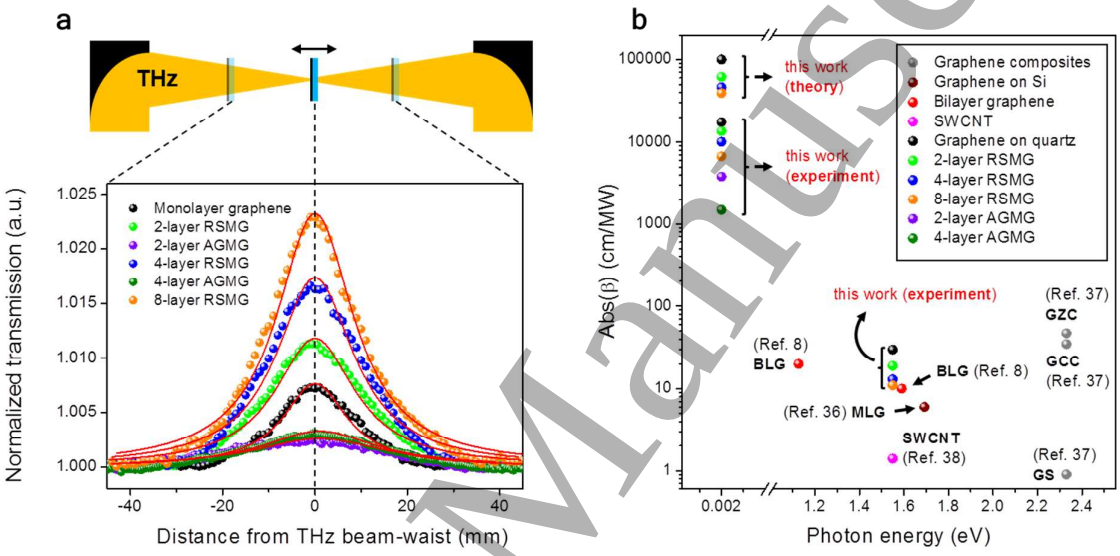

Figure 3. THz nonlinear absorption coefficients of AGMGs and RSMGs and comparison with previous results for other low-dimensional nanocarbons. (a) Experimental results on THz open-aperture z-scan measurement of monolayer graphene, AGMGs, and RSMGs films, with fit curves (red solids) used to extract nonlinear absorption coefficients (β) at THz frequency. (b) Comparison of absolute β values with other low-dimensional nanocarbons in a wide frequency range from THz to the near-infrared region. Black, green, blue, orange, purple, and brown dots represent our experimental and theoretical values for six different samples, monolayer graphene and 2-, 4-, and 8-layer RSMGs and 2- and 4-layer AGMGs, respectively. MLG: monolayer graphene on Si substrate, BLG: undoped bilayer graphene with Bernal stacking, GS: graphene suspension, GCC: graphene-copper porphyrin composite, GZC: graphene-zinc porphyrin composite, GOS: graphene-oxide suspension, SWCNT: single-walled carbon nanotube. Note that the three values in *Ref. 37* were obtained by optical limiting phenomena using nanosecond pulses.

5. Methods

Sample preparation: For this experiment, monolayer graphene was synthesized by CVD on Cu foils using a similar technique to the one reported in *Ref. 39*. The carbon atoms are deposited from a

methane/hydrogen gas mixture on Cu domains at a 1000°C heating temperature, and they are linked to each other on the Cu foil by rapid cooling. We subsequently used the polymer-assisted transfer technique to replace the Cu foil with a quartz substrate. After spin-coating of polymethyl-methacrylate (PMMA) in chlorobenzene on well-grown monolayer graphene, the underlying Cu foil was etched away by 0.5 M aqueous $FeCl_3$ solution. The monolayer graphene on quartz was obtained by scooping up the floating graphene layer and rinsing the supporting PMMA layer with acetone. For the fabrication of RSMG, additional monolayer graphene was transferred onto the graphene-deposited quartz through an iterative layer-by-layer stacking process.

THz transmission measurement: Electro-optic sampling (EOS) and a pyroelectric power meter (THZ5B-MT-DZ, Gentec-EO) were used to measure the time trace of THz electric fields and THz average powers, respectively. Quasi single-cycle sub-picosecond broadband THz pulses serving as the light source were generated by optical rectification in $LiNbO_3$ using a Ti:sapphire regenerative amplifier operating at 1 kHz. The central frequency and spectral bandwidth of the THz pulses (delivering a maximum average output power of 4.3 mW) were 0.6 THz and 1 THz, respectively. The THz beam waist between the two off-axis parabolic mirrors was 1 mm, measured by a pyroelectric camera (PyroCAM-III, OPHIR). We varied the THz pump energy fluence at the sample position from 7.2 nJ/cm^2 to 85.5 μJ/cm^2 using a gold wire-grid polarizer pair with a dynamic range of approximately 40 dB.

6. Conclusion

In summary, the unique nonlinear optical characteristics of RSMG have been systematically investigated in the THz frequency range in comparison with AGMG. The large-area RSMGs, easily fabricated through layer-by-layer stacking of high-quality monolayer graphene and preserving the intrinsic optical characteristics of monolayer graphene, show controllable nonlinearity with substantial enhancements in the transmission modulation of up to a factor of more than four compared to that of AGMG and three orders of magnitude larger THz nonlinear absorption coefficients than those

achieved in the near-IR region. This significant boosting of THz nonlinearities in RSMGs originates from the effective switching-off of the interlayer coupling between graphene sheets and the subsequent superposition of the Dirac-fermionic electronic band of graphene. The fluence-dependent nonlinear THz transmission can be well explained by a thermo-modulational feedback mechanism originating from the ultrafast free carrier heating and carrier-phonon collisions. These results, including enormously large THz nonlinearity and its easy controllability by the layer-by-layer stacking process, make RSMGs highly suitable candidates for a variety of applications in graphene-based THz nonlinear photonic devices.

Acknowledgements

This work was supported by the National Research Foundation (NRF) of Korea funded by Ministry of Science, ICT and Future Planning (MSIP) (2016R1A2A1A05005381 and 2014R1A2A1A11049467), the World Class Institute (WCI) program of the National Research Foundation (NRF) of Korea funded by MSIP (WCI 2011-001) and the Center for Advanced Meta-Materials (CAMM) funded by the Korean government (MSIP) as a Global Frontier Project (CAMM-2014M3A6B3063709). J.M.H, S.S.O., and O.H. acknowledge support from the Leverhulme Trust (UK) and the Engineering and Physical Sciences Research Council (UK).

I H Baek, J M Hamm, and K J Ahn contributed equally to this work.

Competing financial interests

The authors declare no competing financial interests.

References

[1] Castro Neto A H, Guinea F, Peres N M R, Novoselov K S, Geim A K. 2009 *Rev. Mod. Phys.* **81** 109

[2] Li Z Q, Henriksen E A, Jiang Z, Hao Z, Martin M C, Kim P, Stormer H L and Basov D N 2008 *Nat. Phys.* **4** 532-535

[3] Horng J *et al* 2011 *Phys. Rev. B* **83** 165113

[4] Bonaccorso F, Sun Z, Hasan T and Ferrari A C 2010 *Nat. Photonics* **4** 611-622

[5] Ju L *et al* 2011 *Nat. Nanotechnol.* **6** 630-634

[6] Bao Q, Zhang H, Wang Y, Ni Z, Yan Y, Shen Z X, Loh K P and Tang D Y 2009 *Adv. Funct. Mater.* **19** 3077-3083

[7] Xing G, Guo H, Zhang X, Sum T C and Huan C H A 2010 *Opt. Express* **18** 4564-4573

[8] Yang H, Feng X, Wang Q, Huang H, Chen W, Wee A T and Ji W 2011 *Nano Lett.* **11** 2622-2627

[9] Lim G K, Chen Z L, Clark J, Goh R G S, Ng W H, Tan H W, Friend R H, Ho P K H and Chua L L 2011 *Nat. Photonics* **5** 554-560

[10] Wang J, Hernandez Y, Lotya M, Coleman J N and Blau W J 2009 *Adv. Mater.* **21** 2430-2435

[11] Hong SY , Dadap J I, Petrone N, Yeh P C, Hone J and Osgood Jr. R M 2013 *Phys. Rev. X* **3** 021014

[12] Margulis V A, Muryumin E E and Gaiduk E A 2013 *J. Phys.: Condens. Matter* **25** 195302

[13] George P A, Strait J, Dawlaty J, Shivaraman S, Chandrashekhar M, Rana F and Spencer M G 2008 *Nano Lett.* **8** 4248

[14] Khurgin J B 2014 *Appl. Phys. Lett.* **104** 161116

[15] Dawlaty J M, Shivaraman S, Strait J, George P, Chandrashekhar M, Rana F, Spencer M G, Veksler D and Chen Y 2008 *Appl. Phys. Lett.* **93** 131905

[16] Mak K F, Ju L, Wang F and Heinz T F 2012 *Solid State Commun.* **152** 1341-1349

[17] Bianco F *et al* 2016 *Opt. Express* **23** 11632

[18] Wright A R, Xu X G, Cao J C and Zhang C 2009 *Appl. Phys. Lett.* **95** 072101

[19] Paul M J, Chang Y C, Thompson Z J, Stickel A, Wardini J, Choi H, Minot E D, Norris T B and Lee Y S 2013 *New. J. Phys.* **15** 085019

[20] Hwang H Y, Brandt N C, Farhat H, Hsu A L, Kong J and Nelson K A 2013 *Phys. Chem. B* **117** 15819-15824

[21] Luican A, Li G, Reina A, Kong J, Nair R R, Novoselov K S, Geim A K and Andrei E Y 2011 *Phys. Rev. Lett.* **106** 126802

[22] Kim K *et al* 2012 *Phys. Rev. Lett.* **108** 246103

[23] Huang P Y *et al* 2011 *Nature* **469** 389-392

[24] Biró L P and Lambin P 2013 *New. J. Phys.* **15** 035024

[25] Lee E J *et al* 2015 *Nat. Commun.* **6** 6851

[26] Ferrari A C *et al* 2006 *Phys. Rev. Lett.* **97** 187401

[27] Ferrari A C and Basko D 2013 *Nat. Nanotechnol.* **8** 235-246

[28] Das A *et al* 2008 *Nat. Nanotechnol.* **3** 210-215

[29] Yan H, Xia F, Zhu W, Freitag M, Dimitrakopoulos C, Bol A A, Tulevski G and Avouris P 2011 *ACS Nano* **5** 9854-9860

[30] Parret R, Paillet M, Huntzinger J R, Nakabayashi D, Michel T, Tiberj A, Sauvajol J L and Zahab A A 2012 *ACS Nano* **7** 165-173

[31] Wu Y *et al* 2012 *ACS Nano* **6** 7731-7738

[32] Ohta T, Bostwick A, Seyller T, Horn K and Rotenberg E 2006 *Science* **313** 951-954

[33] Lin I T and Liu J M 2014 *IEEE J. of Sel. Top. Quan. Electron.* **20** 8400108

[34] Shi S F, Tang T T, Zeng B, Ju L, Zhou Q, Zettl A and Wang F 2014 *Nano Lett.* **14** 1578-1582

[35] Yin M, Li H P, Tang S H and Ji W 2000 *Appl. Phys. B* **70** 587-591

[36] Chen W *et al* 2013 *AIP Adv.* **3** 042123

[37] Krishna M B M, Kumar V P, Venkatramaiah N, Venkatesan R and Rao D N 2011 *Appl. Phys. Lett.* **98** 081106

[38] Kamaraju N, Kumar S, Sood A K, Guha S, Krishnamurthy S and Rao C N R 2007 *Appl. Phys. Lett.* **91** 251103

[39] Kim K S *et al* 2009 *Nature* **457** 706